Aerospace Science and Technology 70 (2017) 549–558

Contents lists available at ScienceDirect

Aerospace Science and Technology

www.elsevier.com/locate/aescte

Optimization and analysis of hypersonic leading edge geometries

W. Schuyler Hinman *, Craig T. Johansen, Patrick E. Rodi

ARTICLE INFO

Article history:
Received 28 June 2017
Received in revised form 2 August 2017
Accepted 28 August 2017
Available online 1 September 2017

ABSTRACT

An aerothermal optimization study of two-dimensional hypersonic leading edge geometries has been performed using both genetic algorithm and particle swarm optimization. The accuracy of a simplified model and a reduced order numerical model was assessed through comparison to simulations of the compressible Navier–Stokes equations performed in OpenFOAM. Specifically, the estimated surface pressure and laminar convective heating distributions have been compared. The simplified model was found to have compromised accuracy in regions of high and low surface curvature. The reduced order numerical model was found to give accurate results with significantly reduced computational cost compared to complete Navier–Stokes simulations. Optimizations were then performed using the simplified analysis technique, and the reduced order numerical model. The performance of the optimized hypersonic leading edge geometries was analyzed using OpenFOAM. The results show that both methods achieve a similar geometric result. However, the quality of the optimization is improved by using the reduced order numerical model. An analysis was performed in the design space immediately surrounding the optimized geometry to assess the impact of small geometric changes on aerothermal performance. The results show that even small changes in leading edge geometry can have a significant influence on aerothermal performance.

1. Introduction

High lift-to-drag ratio (L/D) supersonic and hypersonic bodies are designed to have sharp leading edges in order to minimize drag [1–8]. However, sharp leading edges are limited by both manufacturability and by excessive convective heating loads at high Mach number. It is known that laminar convective heating can be reduced by increasing the bluntness of the leading edge, as stagnation point heating obeys an inverse relationship with the square of the local body radius at the stagnation point [9]. However, it is a concern for the designers of high speed flight vehicles that blunt leading edge effects could adversely impact the aerodynamic performance of the vehicle. Vehicle drag is increased by the detached bow shock induced by a blunt leading edge. Waveriders, in particular, depend on leading edge shock attachment to their forward surface in order to contain the high pressure air that produces efficient lift. Waverider performance is thus very sensitive to the shape of the finite leading edge. Additionally, the shape of the blunt leading edge determines the stream-wise pressure gradient and therefore can adversely impact the stability of the laminar boundary layer. Both the drag and heating reductions associated with a laminar boundary layer design can be significant.

General studies of what constitutes aerodynamically “sharp” vs. “blunt” leading edge geometries for high speed vehicles have been conducted [10]. Specific to waverider-based vehicle configurations, the impacts from hemi-cylindrical and power-law body leading edges on performance have been examined [11–16]. O'Brien and Lewis [12] employed power-law curve finite leading edge geometries and showed blunt body-like pressure gradient behavior very close to the stagnation point. Vanmol and Anderson [15] examined the heat transfer to hypersonic waveriders, with an emphasis on effects caused by the finite leading edge. They incorporated a hemi-cylindrical leading edge blunting technique, with the local leading edge radius as a function of spanwise position.

Studies [17–23] have been performed regarding finite leading edge geometries using power law curves and Bezier Curves. These include both two-dimensional and axisymmetric configurations, using various optimization schemes. Additionally, the related problem of optimizing re-entry heat shields has also been explored [24–27]. These studies show that the convective heating and/or the drag of the leading edge can be reduced via shaping. The optimized shapes are relatively invariant to both Mach and Reynolds number changes. These trends indicate that any optimized configuration would represent a robust solution for the vehicle designer, having the potential to provide an advantage over a range of conditions. Optimized geometries generated using simplified methods or full Navier–Stokes analysis appear to be qualitatively very sim-

* Corresponding author.
E-mail address: wshinman@ucalgary.ca (W.S. Hinman).

http://dx.doi.org/10.1016/j.ast.2017.08.034
1270-9638/

Nomenclature

$a_1 \ldots a_n$	NASA polynomial coefficients	St	Stanton number
C	Sutherland's constant	T	Temperature (K)
C_1, C_2, C_3	Empirical constants for Kays laminar heating method	U	Velocity magnitude (m/s)
C_p	Coefficient of pressure	θ	Flow deflection angle (°)
c_p	Constant pressure specific heat capacity (J/kg·K)	κ	Thermal conductivity (W/m·K)
c_v	Constant volume specific heat capacity (J/kg·K)	μ	Viscosity (N·s/m^2)
H	Total enthalpy (J/kg), Leading edge height (m)	μ_o	Sutherland's reference viscosity (N·s/m^2)
P	Pressure (Pa)	ρ	Density (kg/m^3)
q_∞	Free-stream dynamic pressure (Pa)	ϕ	Angular leading edge coordinate (°)
q''	Wall heat-flux (W/m^2)	*Subscripts*	
R	Axi-symmetric body radius (m)	aw	Adiabatic wall properties
R_g	Gas constant (J/(kg·K))	e	Boundary layer edge properties (N·s/m^2)
r	Radius of curvature (m)	e	Wall properties
S	Sutherland's constant	∞	Free-stream properties
R_g	Entropy (J/K)		

ilar. However, the accuracy of using simplified methods to assess the performance of these geometries is not well understood.

In recent work, genetic algorithm (GA) and particle swarm optimization (PSO) was used to optimize a leading edge for heat transfer and pressure drag reduction [18,22]. Bezier curves were utilized due to the increased geometric flexibility available compared to power-law based geometries. The study by Rodi [18] produced an optimized shape resulting in a decrease in laminar convective heating of 23.4% and an increase in pressure drag of 17.1% for the hypersonic laminar conditions investigated. The optimization utilized simplified analysis techniques for the prediction of drag and convective heating. It is of interest to investigate the effect of using simplified analysis techniques on the optimization.

In general, the effectiveness of any optimization routine is limited by the accuracy of its model. An optimization routine executed up to a high precision could still have a less than desirable accuracy. The design space being explored must reflect the region where the analysis technique is sufficiently accurate. Failure to do so could result in non-physical or artificial minima. Additionally, within an appropriate design space, due to reduced accuracy in response to geometric changes, the location of local and global minima may change. Consequently, this question is a major focus of the present work. Do the locations of the minima change due to an increase in physical accuracy?

In addition to the accuracy of the physical model, computational cost is an important concern. In general, Computational Fluid Dynamics (CFD) simulation of the compressible Navier–Stokes equations offers the most robust and accurate means of studying a high speed flow problem numerically. However, the expensive nature of the Navier–Stokes equations can often make them unsuitable for optimizations with a relatively large and/or complicated design space. Efforts in areas such as surrogate-based modeling and adjoint optimization have been made to reduce the number of CFD simulations necessary. In the surrogate-based modeling approach, a set number of simulations is performed and the gaps in the design space are filled in with an appropriate model [28]. This model is then used to perform the objective function evaluations during the optimization and can be combination of high and low fidelity methods [29,30]. Adjoint optimization is a form of gradient based optimization where the CFD solver is modified to produce the sensitivities of the objective function to the design variables directly. This reduces the number of simulations required compared to perform a gradient based optimization where finite differences are used to compute the sensitivities [31,32]. However, despite the advantages posed by these approaches, in complicated design spaces including multiple design points and objectives there is significant value in reducing the cost per simulation. Often, a sacrifice in grid resolution for the simulation is made [33]. Alternatively simplified analysis techniques can be used. However, as stated, the effect of using reduced fidelity modeling on the optimized results is unclear and is a motivation for this work.

In the present work, applications of a simplified analysis technique, numerical solutions to the Euler equations plus the boundary layer equations, and simulations of the compressible Navier–Stokes equations are compared. A code developed for analyzing blunt body flows (HyPE2D) is used as an intermediate fidelity analysis tool. The accuracy from three different analysis techniques are compared for a few representative leading edge geometries. An optimization is performed with both the simplified analysis technique (referred to, from here on, as the Newton–Kays model) and HyPE2D. The aerothermal performance of the optimized geometries is analyzed using rhoCentralFOAM (regarded as the benchmark for accuracy in this study) and compared to the lower fidelity models.

2. Performance analysis details

2.1. Simplified analysis details (Newton–Kays model)

The fastest analysis technique used here is a combination of a simple model for the inviscid external flow, and an integral approach to the laminar boundary layer heat transfer. These are typical engineering style approaches that are highly useful early in a design process but are often supplanted by more sophisticated techniques when more accurate results are required.

2.1.1. Modified Newtonian method

The modified Newtonian method is a simple analytical tool based on the body inclination angle and a prediction of the maximum pressure coefficient in the shock-layer [9]. The calculation is given in Equations (1) and (2).

$$C_p = C_{p,max} \sin^2 \theta \tag{1}$$

where:

$$C_p = \frac{p - p_\infty}{0.5 \rho U_\infty^2} \tag{2}$$

Here, $C_{p,max} = 1.8316$ is found using the normal shock relations to calculate the stagnation pressure behind the fore-body shock assuming constant specific heats. The flow deflection angle θ is the difference between the body surface inclination angle and the

angle of the oncoming free-stream flow. Once the pressure distribution along the surface is known, the other flow parameters (T, U, ρ) along the body are calculated using the isentropic flow relations.

2.1.2. Kays laminar heating method

Once the inviscid flow properties are known, the Kays laminar heating method [34] is used to calculate the distribution of the Stanton number (St) around the leading edge. The calculation is given in Equation (3).

$$St = \frac{C_1 \mu^{0.5} R G_e^{C_2}}{(\int_0^x G_e^{C_3} R^2 dx)^{0.5}} \left(\frac{T_s}{T_e}\right)^{-0.08} \left(\frac{T_{aw}}{T_e}\right)^{-0.04} \tag{3}$$

Here, $G_e = \rho u_e$, μ is the viscosity (evaluated at film temperature), and C_1–C_3 are empirical constants ($C_1 = 0.418$, $C_2 = 0.435$, $C_3 = 1.87$). R is the axisymmetric body radius and cancels out of the equation in the two-dimensional case as in this study.

2.2. HyPE2D simulation details

Fast and accurate design tools offer significant advantages over both highly simplified approaches and high quality CFD when applied to optimization design problems. Simplified approximations typically suffer from decreased accuracy, whereas CFD suffers from high computational cost. HyPE2D is a fast and accurate simulation tool for solving two dimensional hypersonic flow over blunt bodies [35]. HyPE2D was developed using the shock-fitting principles outlined by Salas [36] and the boundary layer modeling described by Schetz [37]. The solution in the present work is solved assuming that there is no significant viscous-inviscid interaction. However, a correction for viscous-inviscid interactions is easily applicable for low Reynolds number cases as has been performed in a related study pertaining to the expanding flow on the aft-body of a circular cylinder [35]. In the present formulation, a result for the flow-field is achieved on a personal computer in approximately 100 seconds. The speed of the solution varies with geometry, boundary conditions and grid resolutions. The grid resolutions used to solve the Euler equations, and the boundary layer equations, in the subsequent optimization routines were selected to balance accuracy and computational time. Sufficient accuracy is required to correctly guide the optimization, but fast enough solution time is necessary for the process to remain feasible. The working grids were used in the comparison shown in Section 3 and gave adequate results, as well as an acceptable solution time.

2.2.1. Inviscid flow (Euler equations)

HyPE2D solves the inviscid flow using the shock-fitting principles outlined in the textbook by Salas [36]. A finite difference grid is generated between the leading-edge body and an empirically estimated initial bow shock-wave location. The grid is then transformed to a rectangular grid through a coordinate system transformation. A typical grid is shown in Fig. 1 for a geometry from Rodi [18]. The unsteady modified Euler equations are solved on the grid using the MacCormack method [9,36]. At each step forward in pseudo-time, the location of the shock and the flow properties behind it are updated. The solution is progressed until the field is converged to an acceptable level (wall temperature distribution converged to 1×10^{-3}%). Equilibrium properties are recalculated at each time-step using the thermo-physical models outlined in Section 2.4, and are used to calculate the jumps across the shock boundary. The shock-wave is solved numerically using the shock-jump conservation equations. The solution for these equations is achieved iteratively using the Newton–Raphson method for solving non-linear systems of equations.

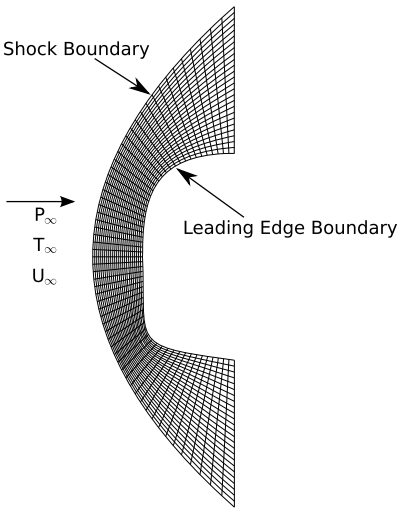

Fig. 1. Typical HyPE2D Shock-Fitted Grid.

2.2.2. Viscous flow (boundary layer equations)

The viscous flow is solved numerically using the approach outlined by Schetz for solving non-similar compressible boundary layers [37]. The location of the stagnation point, as well as the properties along the body are taken from the inviscid flow solution described in Section 2.2.1. The initial velocity and enthalpy profiles are calculated at the stagnation point using the similarity solution outlined by Cohen and Reshotko [38]. The solution is then marched forward in the stream-wise direction away from the stagnation point along the upper and lower surface of the leading edge using a semi-implicit Crank–Nicholson method. The gas specific heats (c_p, c_v), viscosity (μ), and thermal conductivity (κ) are calculated at each stream-wise step using the models in Section 2.4.

2.3. OpenFOAM simulation details

2.3.1. Compressible flow solver

Two-dimensional Navier–Stokes simulations were performed using the open-source software, OpenFOAM [39]. Specifically, the high speed flow solver rhoCentralFoam was used in the simulation. The solver rhoCentralFoam is a density based solver of the unsteady, compressible Navier–Stokes equations [40]. RhoCentralFoam has been shown to give close agreement to experimental data for similar high-speed flows. For example, Arisman et al. [41,42] showed close agreement to both experimental results and results from a common commercial solver. Wall pressure distributions were compared for flow over a supersonic circular cylinder by Hinman and Johansen [43]. In this case, the numerical prediction was found to be within the experimental error. Teh and Johansen [44] successfully validated rhoCentralFoam for supersonic shockwave boundary layer interactions. In the works of Li et al. [45,46], rhoCentralFoam was used to simulate an under expanded jet using LES turbulence modeling. In those studies, the simulation results were compared to experiments and showed close agreement. Reichel and Groll [47] performed a rigorous comparison of rhoCentralFoam results to pressure data obtained from flow over three different double cone geometries and showed good agreement between the numerical solution and experiment. As well, synthetic Schlieren was compared to the Schlieren photographs captured in the experiment and showed qualitative agreement.

2.3.2. Geometry and boundary conditions

The flow-field around each Bezier Curve Leading Edge (BCLE) was meshed using the OpenFOAM native meshing software,

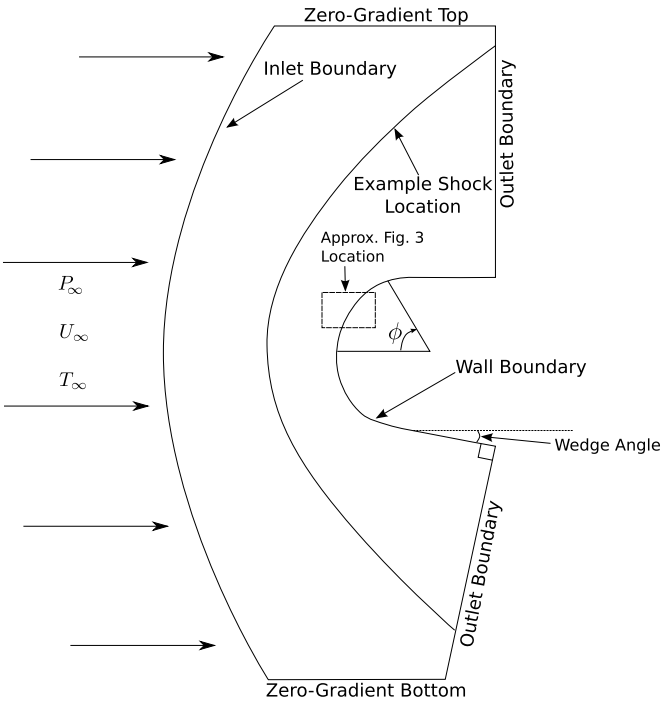

Fig. 2. Schematic of OpenFOAM simulation geometry.

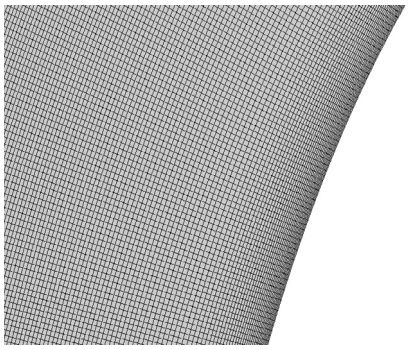

Fig. 3. Typical mesh close to wall (see Fig. 2 for location).

blockMesh. A schematic of the domain geometry and boundary conditions are shown in Fig. 2. The domain was generated in such a way so as to allow mesh clustering near the shock wave, and clustering of cells in the boundary layer. The outlet boundary on the lower surface of the leading edge was generated on an angle to ensure adequate orthogonality of the cells along the leading edge surface. Grid convergence was checked for the rhoCentralFoam simulations using Richardson extrapolation for peak heat flux, and integrated heat flux. The refined grids typically resulted in less than 0.5% error (with grid convergence index < 0.5) in peak convective heat flux from the Richardson extrapolation prediction. This result was achieved through high grid resolution in the boundary-layer and at the bow shock. The maximum y^+ value in the refined grids was maintained at < 0.05 and the maximum cell Reynolds number was maintained at < 2. A close-up of a typical computational grid close to the wall is shown in Fig. 3.

The simulation inlet conditions are specified with free-stream static pressure ($p_\infty = 1365.78$ Pa), static temperature ($T_\infty = 225.636$ K), and velocity ($U_\infty = 3014$ m/s). These inlet conditions correspond to a Mach number of $M = 10$, and a free-stream dynamic pressure of $q_\infty = 9.57604 \times 10^4$ Pa (2000 psf) as used in the previous work by Rodi [18,22]. The wall of the leading edge is specified with a constant wall temperature ($T_w = 311$ K), and the no slip condition for velocity. The wall temperature was chosen to be consistent with previous work [18,22]. In those works, 311 K was chosen to reliably produce accurate cold wall heating distributions, ensure numerical stability, and minimize its effect on the optimized solution. Depending on the level of active cooling at the leading edge, the choice of wall temperature is somewhat arbitrary. All outlet boundaries are specified with a zero-gradient boundary condition for all properties. This treatment is suitable as long as the flow is supersonic at the boundary [9]. The field is initialized with a zero velocity field at the free-stream static pressure and static temperature. The steady state solution of the flow-field is then achieved by marching forward in time until changes in the properties of the flow field are negligible.

2.4. Thermophysical properties

In order to account for the large temperature changes in the simulation, the fluid's thermodynamic properties are modelled. The gas specific heats are modeled using a 7-coefficient NASA polynomial for JANAF thermophysical data [48]. The polynomials are given in Equations (4) to (6).

$$c_p = R_g\left(a_1 + a_2 T + a_3 T^2 + a_4 T^3 + a_5 T^4\right) \tag{4}$$

$$H = R_g T\left(a_1 T + a_2 T^2/2 + a_3 T^3/3 + a_4 T^4/4 + a_5 T^5/5 + a_6\right) \tag{5}$$

$$S = R_g\left(a_1 \ln T + a_2 T + a_3 T^2/2 + a_4 T^3/3 + a_5 T^4/4 + a_7\right) \tag{6}$$

The viscosity is modelled using Sutherland's law [9,49] shown in Equation (7).

$$\mu = \mu_o \frac{T_o + C}{T + C}\left(\frac{T}{T_o}\right)^{3/2} \tag{7}$$

The thermal conductivity can also be modelled using Sutherland's law, but for these calculations it is modelled using the modified Eucken Method given in Equation (8). Here c_v is the constant volume specific heat capacity, and R_g is the specific gas constant.

$$\kappa = \mu c_v\left(1.32 + \frac{1.77 R_g}{c_v}\right) \tag{8}$$

3. Comparison of flow-field predictions

Analysis has been performed at the properties described in Section 2.3.2 for a selected arbitrary test geometry. Fig. 4 shows Mach number isolines for the geometry shown in Fig. 1. The geometry was intentionally selected to test the accuracy of the HyPE2D flow simulation and the Newton–Kays model compared to rhoCentralFoam. This geometry is an appropriate test case due to its relatively high curvature corners, and low curvature in the vicinity of the stagnation point. We can see that both results show good qualitative agreement, with little noticeable difference between the two flow-fields.

The predicted laminar heat flux for the BCLE has been compared in Fig. 5 for the three different analysis techniques described in Section 2. The quality of the results found from HyPE2D is evident due to the close agreement with OpenFOAM. The locations of the peaks in wall heat flux distribution coincide closely and the magnitudes are only marginally over-predicted. A major deficiency of the Newton–Kays model (Section 2.1) is seen at the regions with either significantly high curvature or low curvature. The curvature is low close to the stagnation point and this results in a significant under-prediction of the local wall heat flux. Around the corners where the curvature is high, the heat transfer is over-predicted. However, the Newton–Kays model correctly approximates the qualitative response to changes in local curvature and pressure gradient. A major deficiency of both HyPE2D and the

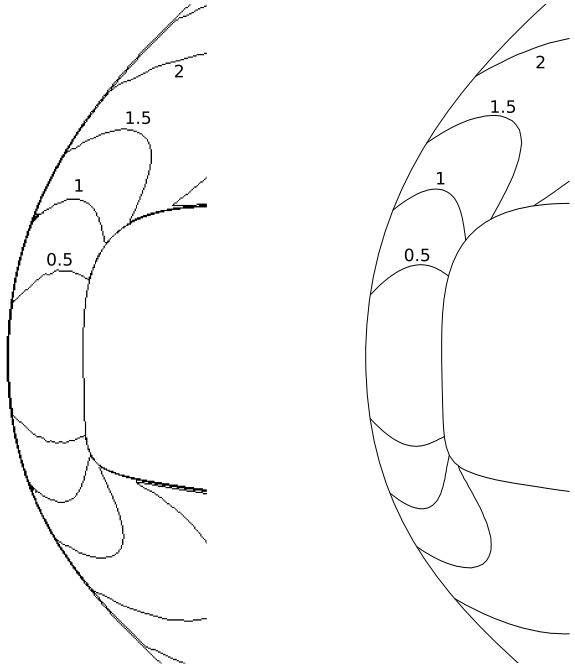

Fig. 4. Mach number iso-lines using rhoCentralFoam (Left) HyPE2D (Right).

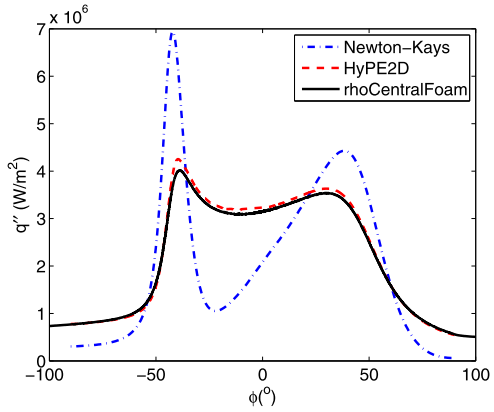

Fig. 5. Comparison of predicted wall heat flux (W/m^2) distribution.

Newton–Kays model is the poor performance close to the stagnation point. This poor performance is due to the presence of a streamwise dimension close to zero (for example, the integral in the denominator of Equation (3) is zero at the stagnation point). In order to obtain smooth data in this region using HyPE2D, a very fine discretization in the stream-wise direction is required. Therefore in both of these methods, the region very close to the stagnation point ($\phi = \pm 5°$) is interpolated through from points outside this region, yielding smooth results.

Predictions for pressure distribution along the BCLE surface are compared in Fig. 6. The surface pressure distribution is important for the prediction of drag, as well as the effect of the shape on the stability of the laminar boundary layer. The predicted pressure distributions show reasonable qualitative agreement between all three analysis methods. However, the predicted gradients in pressure around the sharp corners are exaggerated by the modified Newton's method. A deficiency of the Newton–Kays model is it's inability to accurately predict the post-shock stagnation pressure. The value of $C_{p,max}$ is calculated using frozen gas properties (constant specific heats) which affects the post-shock properties. While the value of $C_{p,max}$ could be corrected by performing an equilibrium shock calculation, the primary deficiency of the method is

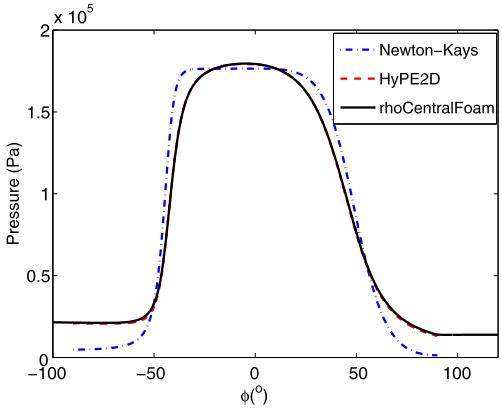

Fig. 6. Comparison of predicted pressure (Pa) distribution.

with the modified Newton's method itself, not the specific value of $C_{p,max}$. The predicted pressure distributions from HyPE2D and rhoCentralFoam match closely. This agreement indicates that for these flow conditions, the assumption that the boundary layer does not significantly impact the inviscid flow is valid. Additionally, the adequate accuracy of the numerical solution to the equilibrium jump equations is indicated by the closely matching stagnation point pressure.

The comparison of the predictive methods raises important questions about the applicability of the Newton–Kays model for a shape optimization routine. In the present study, and in previous work [18,22], Bezier curves were utilized. Employing Bezier Curves is a versatile method for using a small number of input variables to generate a wide variety of geometries that are continuous and differentiable [50–52]. Consequently, these attributes make them attractive for use in aerospace optimization problems. However, a more robust physics model is required in order to accurately account for increased geometric complexity. For example, the Bezier curve approach allows for geometries that incorporate local regions of high and low curvature. We have seen here that the modified Newton's method, when coupled with Kays laminar heating, results in decreased accuracy in both of these cases. Thus, it is possible that when an optimization objective function requires evaluation of either a low or high curvature geometry, the optimized result will be unsatisfactory using the Newton–Kays model. For such a case, attention should be paid to limiting the design space to ensure accuracy. Additionally, an important consideration when using Newton–Kays model is the quality of the analysis itself. For example, in the best case, the Newton–Kays model may arrive at the same optimized geometry as a more sophisticated analysis. However, a designer must then check the result in order to avoid over-predicting any performance benefits of the new geometry, or failing to predict changes in flow-field topology such as boundary layer separation or turbulent transition. Some of these points are discussed in Section 4 using the current optimization results.

4. Peak heat flux minimization

Optimizations were performed to achieve a minimum peak wall heat flux on the leading edge of an 8 degree wedge. The leading edge geometries are generated by changing the location of 4 Bezier curve control points. Optimizations were performed using both GA and PSO. The GA in Matlab's Optimization Toolbox [53], and a user contributed particle swarm toolbox were used in this work. Repeating the optimization process with different minimization algorithms resulted in increased confidence in the result. Additionally, this process provided insight into which algorithm was best suited to the problem based on convergence performance. In

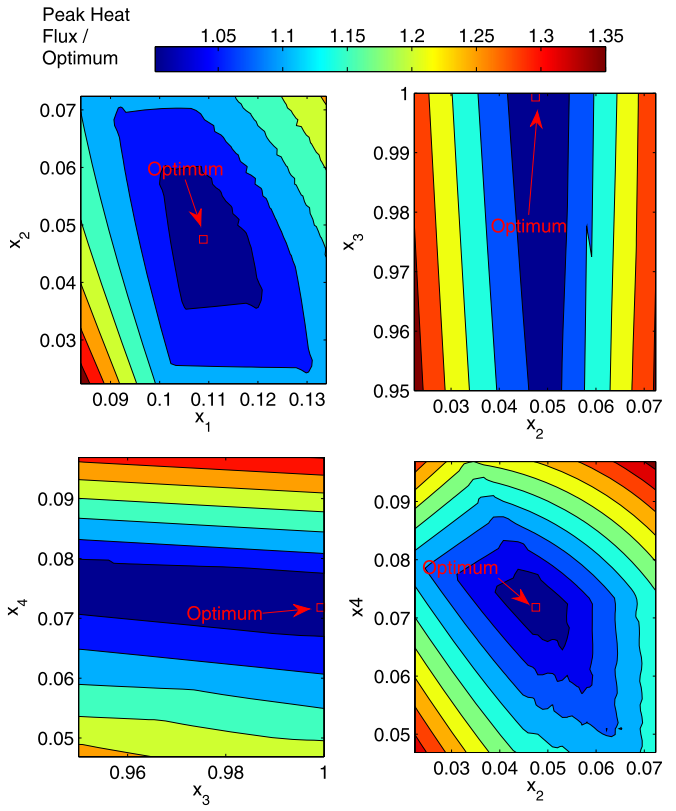

Fig. 7. Contour plots of the peak heat flux value across the design space. (For interpretation of the references to color in this figure, the reader is referred to the web version of this article.)

order to keep the geometries physically realistic, a penalty function was used to limit the resulting geometries to have a similar cross-sectional area for a Hemi-Cylindrical Leading Edge (HCLE). The objective function for geometries with a cross-sectional area beyond ±1% of that of a HCLE were penalized. This penalty function was also used by Rodi in his previous optimization study [22].

4.1. Solution topology

The ability to rapidly generate solutions from either the engineering-based Newton–Kays approach or the Euler-based HyPE2D approach offers the opportunity to explore the design space of this problem in detail. For both approaches a 4-variable design space was utilized. Within this space, the optimization function was defined as the peak of the heat flux distribution. By examining the behavior of this peak heat flux value across the design space, one can make a number of observations about the applicability of certain classes of optimizers to this problem.

A large number of cost function evaluations were made, using the Newton–Kays model, to systematically explore the design space in detail. Currently, four independent variables (x_1–x_4) are used to define the shape of the candidate BCLE. The matrix of Newton–Kays results consisted of 10,000 unique revaluations and the peak heat flux values are illustrated using a series of contour plots in Fig. 7.

In these contour plots the peak heat flux value is normalized by the optimal result. From these contour plots, the observation is made that for this problem the minimum peak heat flux value lies within a larger floor of similarly valued solutions. Additionally, the walls around the floor appear to be well behaved for use with a Gradient Descent (GD) optimization scheme. However, a more detailed examination of the solution data indicates that such a conclusion may be optimistic.

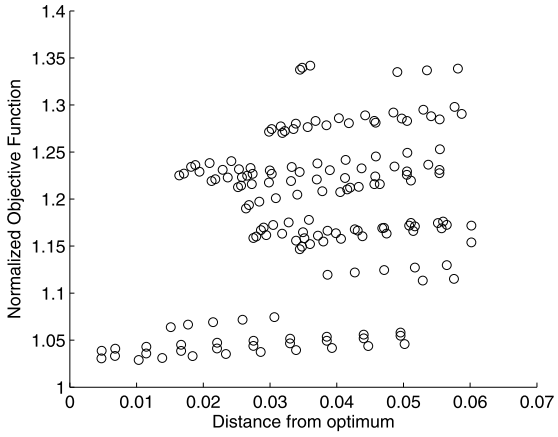

Fig. 8. Distribution of locations with problematic gradient descent information.

GD optimization approaches require consistent gradient direction and magnitude to successfully reach the desired optimum. GD optimizers can be confused by solution waviness or even numerical noise in the cost function data [32]. Various modifications have been used to improve the performance of GD optimizers in such situations. However, a universal approach is not available and reaching the global optimum is not guaranteed. After examining the solution space, 160 unique occurrences were identified where the direction of the solution gradient was not in the general direction of the final optimum solution. Using the formula,

$$\cos\theta = \frac{\vec{A}\cdot\vec{B}}{|\vec{A}||\vec{B}|} \tag{9}$$

where $\vec{A}$ is the vector of the local solution gradient, and $\vec{B}$ is the vector from the local location to the optimal solution. Any occurrences where $\cos\theta < 0$, were examples where the local solution gradient vector pointed away from the optimal solution, potentially causing a GD optimizer to proceed in the wrong direction of the solution space. Fig. 8 shows a distribution of these points, plotted against the distance from the optimal solution. In this plot the ordinate has been normalized by the actual optimal value, so the minimum possible value along this axis is unity.

The number and distribution of such points reduces the certainty to below 100% of whether a GD approach would reach the designed optimal value. It is possible that a GD optimizer could reach the global minimum for this case since the density of problematic solution gradient locations is relatively low. In the event that a GD optimizer encountered one of these problematic locations, the use of momentum and velocity limits could allow the GD to proceed in the correct direction. While not proven by the data generated herein, it is possible that an adjoint approach could similarly encounter problems reaching the global minimum. The GA approach does not utilize solution gradient information.

4.2. Peak heat flux minimization using Newton–Kays model

Optimizations were first performed using the Newton–Kays model. A major benefit of this technique is the low computational cost. Consequently, large sample populations can be evaluated for many generations to ensure a highly resolved optimal result. The GA optimizations were performed using a population of 3000 and were run until a convergence of 10^{-6} in the objective function was reached. It was found by the authors that at least in this specific case PSO had better convergence and a population of 200 was used. The results typically converged in less than 400 generations. Optimizations were repeated to ensure that the results

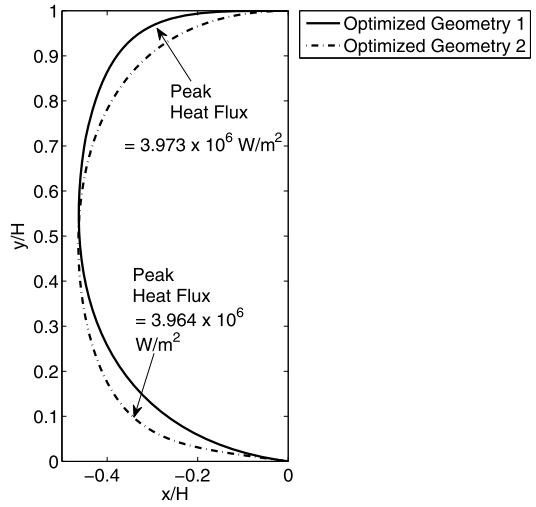

Fig. 9. Optimized geometries using the Newton–Kays model.

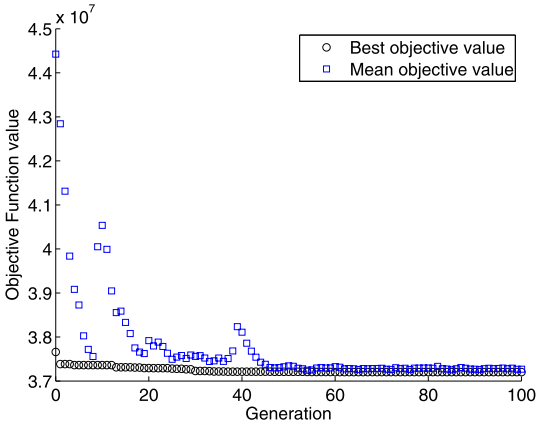

Fig. 11. Typical optimization convergence for GA with HyPE2D.

were correct and not dependent on the choice for the initial population. The non-linear and asymmetrical nature of the problem leads to two possible optimized geometries. One solution involves a reduced radius of curvature corner at the upper surface, and the other involves a reduced radius of curvature corner at the lower surface. The two optimized results are shown in Fig. 9. The two geometries result in nearly the same peak convective heat flux with only a 0.2% difference. The same results were found using PSO. The optimal result with the sharp corner at the upper surface is similar to the geometry found in the previous work performed by Rodi [22] and is therefore the focus of the proceeding analysis.

4.3. Peak heat flux minimization using HyPE2D

HyPE2D offers a significant advantage over full Navier–Stokes simulations in terms of the required computational resources. However, the cost associated with HyPE2D is still much higher than simplified analysis techniques. In order to reduce the time required for the HyPE2D optimizations, the design space was limited to a $\pm 5\%$ (displacement of control-point) region of the design space for each control point encapsulating the optimized result from the optimization using the Newton–Kays model. Additionally, this ensured that the improved optimization was working in the design space close to the previous optimized result. The size of the reduced design space region was chosen arbitrarily and then checked to ensure that the correct peak heat flux minima was in fact located within the design space. Due to difficulties in visualizing the design space in these dimensions, random geometries within the design space were generated and the limits of the space were found in the $X-Y$ plane, and for curvature. The limits of the design space for the HyPE2D optimization are shown in Fig. 10. The flexibility of the design space when using Bezier curves is clear from Fig. 10. By reducing the design space, the optimization was limited to varying the radial dimension close to the stagnation point, and the radius of curvature at the upper surface. The optimization using the HyPE2D flow model was performed using a population of 102 for GA, and 42 for PSO (run in parallel on a 6 processor CPU). The GA was run for 100 generations (10302 unique HyPE2D flow simulations) and the mean change in the fitness function was less than 1%. PSO was run for 200 generations (8400 unique HyPE2D flow simulations) and the mean change in the fitness function was less than 1%. A typical convergence for the HyPE2D optimizations performed is shown in Fig. 11.

The optimized geometries using the Newton–Kays model and HyPE2D are shown in Fig. 12. The improved flow model changes the optimal geometry slightly. A smaller radius of curvature is found at the top, while a larger radius of curvature is found in the vicinity of the stagnation point. Table 1 shows the performance of the two optimized geometries compared to the HCLE. All of the analysis methods show a significant decrease in peak heat flux compared to the HCLE. Both optimization methods have resulted in a leading edge that performs significantly better than the HCLE.

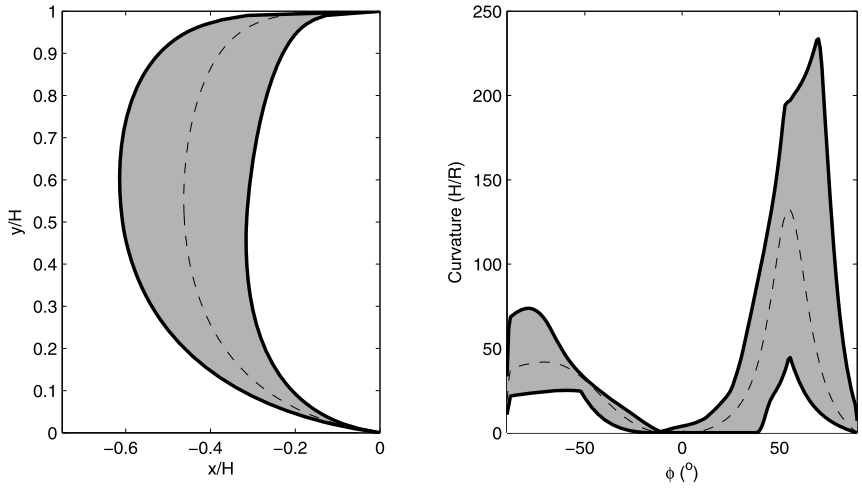

Fig. 10. Approximate design space limits for HyPE2D optimization (dashed line corresponds to optimized shape).

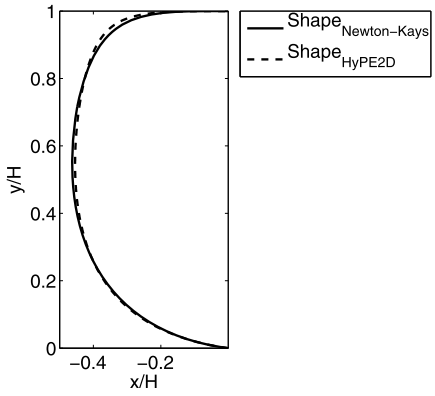

Fig. 12. Optimal leading edge geometries found by various methods.

Table 1
Percent decrease in peak heat flux compared to hemi-cylindrical leading edge.

	N–K	HyPE2D	rhoCentralFoam
$\text{Shape}_{Newton-Kays}$	19.4%	13.6%	14.9%
Shape_{HyPE2D}	14.1%	16.5%	17.9%

However, the shape found using HyPE2D performs slightly better. As is expected the Newton–Kays model predicts a greater decrease in peak convective heat flux for the optimized geometry found using the same method. The predicted heat flux profiles along the leading edge surface are shown in Fig. 13. These profiles show that the different result is due to the Newton–Kays model's over-prediction of convective heat flux in regions of high curvature. This over-prediction means that a more conservative shape is selected when in fact, a higher curvature can be tolerated. Despite this, the Newton–Kays successfully demonstrated that a reduced fidelity can be used to narrow the design space in the present case. However, it should be noted that the effectiveness of this methodology depends on the complexity of the study at hand.

Another important consideration in these optimizations is the increase in drag as a result of the decreased peak convective heat flux. The present study only optimized for minimum peak heat flux, and thus the drag cost was not accounted for. However, it can be shown that even optimizing a BCLE shape at a fixed leading edge height gives a better result than simply optimizing a blunted radius. The pressure drag coefficient was calculated for each geometry using the pressure calculated by rhoCentralFoam. The HyPE2D optimized shape resulted in a pressure drag increase of 8.7%, and the Newton–Kays model optimized shape resulted in an increase of 6.7%. The equivalent HCLE leading edge that would give the same peak heat flux as the optimized geometry. It was found that a 41.8% increase in leading edge height would be required for a HCLE to give the same performance as the optimized geometry. Thus even though the coefficient of drag was increased by 8.7% for the optimized shape, the cost of achieving the same heat flux reduction with a HCLE is a 41.8% increase in drag. An optimization of a BCLE for both drag and heat flux and allowing a variable leading edge height will likely give exceptional results. Future analysis could include a multi-objective optimization for the reduction of both drag and heat flux. The present study agrees with previous work [18,22,23] by showing that higher order shapes can provide a superior means to passively control leading edge flow compared to simple hemi-cylindrical geometries.

4.4. Sensitivity of peak heating to displacement and curvature

In order to examine the relative performance compared to geometries close within the design space, an analysis was performed using random generation of geometries within a significantly reduced design space. The geometries were created by randomly relocating the Bezier curve control points within the design space. Here, approximately 5×10^5 geometries were created and then filtered to only include those within $\pm 1\%$ of the cross-section area of the geometry. This is to ensure consistency between the current method and the genetic algorithm fitness function. After filtering, approximately 36000 geometries that met the area requirement were evaluated and compared against the optimal geometry from Section 4. The random geometries were binned based on their maximum percent difference in radial dimension. Because of the large number of calculations performed in this brute force method, the Newton–Kays model was used for the performance evaluation. In each bin, the mean, maximum and minimum percentage change in peak heat flux was calculated. The results are shown in Fig. 14. It is clear from the results that the optimization has performed well. A small change in the radial dimension results in a significant increase in peak convective heat flux. For example, a 2%–3% uncertainty in the leading edge geometry would result in, at minimum, a 3% increase in peak heat flux. However, it could result in up to a 14% increase, and on average would result in a 7% increase. The relationship between surface geometry imperfections

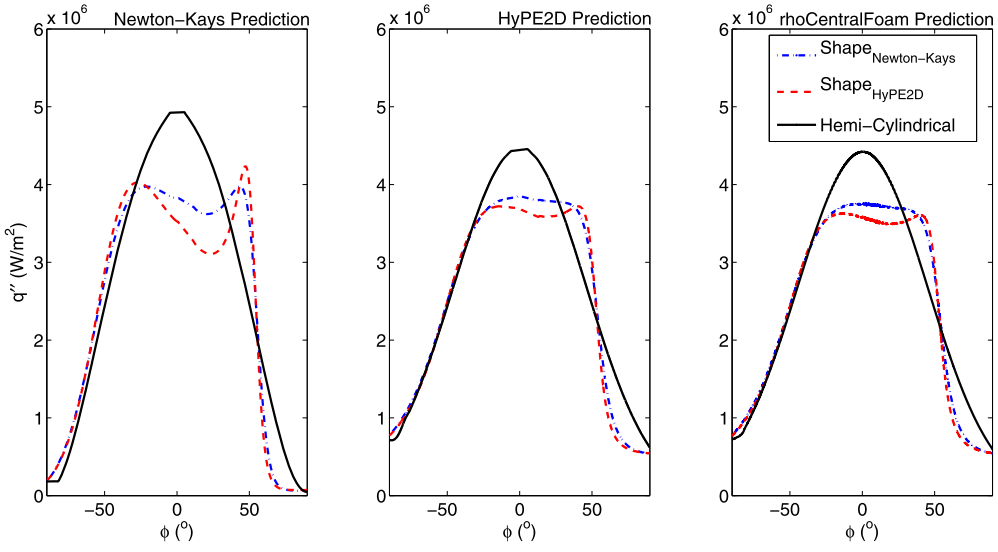

Fig. 13. Heat transfer predictions for the optimized results in Fig. 12.

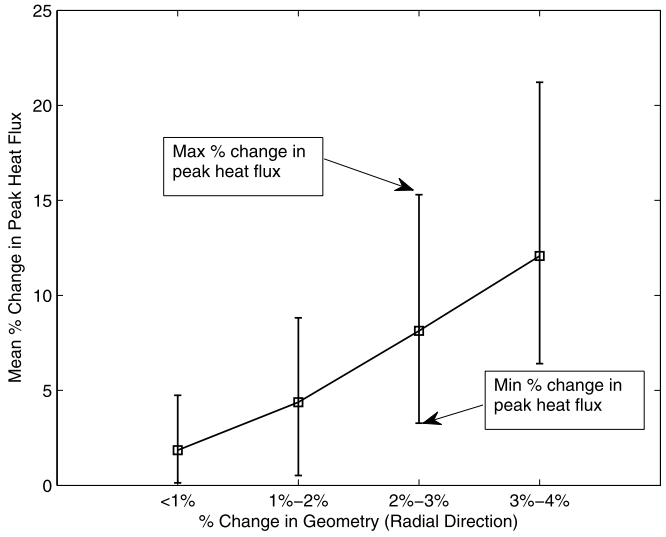

Fig. 14. Relative performance of geometries close within the design space.

and a heat flux penalty could provide the means for a vehicle designer to account for factors such as fabrication tolerances when designing leading edges. For example, in the worst case, a machine tolerance of 10/1000 of an inch in the fabrication of a 1 inch radius leading edge could result in a 5% penalty in the peak heat flux.

5. Conclusion

A simplified model (modified Newton's method with Kays laminar heating) and a new reduced-order model (HyPE2D) were used to optimize the two-dimensional leading edge geometry at Mach 10 based on a peak laminar heat flux. The performance of each model was assessed based on comparisons to fully compressible two-dimensional Navier Stokes simulations using OpenFOAM's rhoCentralFoam solver. HyPE2D showed excellent agreement with the rhoCentralFoam results for both pressure and convective heat flux distributions. However, HyPED2D required the use of the simplified model to initially reduce the size of the design space such that the HyPE2D optimization could complete in a practical amount of time. The simplified model, on its own, failed to accurately predict the surface heat flux in areas of high or low radius of curvature. Despite this deficiency, both models produced a very similar optimized shape. The heat flux of each optimized shape was compared to that of a hemi-cylindrical leading edge geometry using OpenFOAM. The optimized geometry obtained from the simplified model resulted in a 15.5% decrease in peak heat flux and a 6.7% increase in pressure drag. The optimized geometry using HyPE2D resulted in a 17.7% decrease in peak heat flux and a 8.67% increase in pressure drag. An equivalent reduction in peak convective heat flux using an HCLE would result in a 42% increase in pressure drag. Analysis of the design space around the optimal geometry was performed to quantify the sensitivities between small changes in geometry and the associated heat flux penalty. It was found that a significant heat flux penalty ($\approx$5%) can occur, even for very small deviations in the leading edge radius ($<$1%).

Conflict of interest statement

No conflict of interest to declare.

Acknowledgements

This research was enabled in part by support provided by WestGrid (www.westgrid.ca) and Compute Canada Calcul Canada (www.computecanada.ca). Financial support was provided by the Natural Sciences and Engineering Research Council of Canada (NSERC).

Appendix A. Supplementary material

Supplementary material related to this article can be found online at http://dx.doi.org/10.1016/j.ast.2017.08.034.

References

[1] A.J. Eggers, M.M. Resknikoff, D.H. Dennis, Bodies of Revolution Having Minimum Drag at High Supersonic Airspeeds, NACA TN 3666, Tech. Rep., NACA, 1957.
[2] A.J. Eggers, H. Ashley, G.S. Springer, J.V. Bowles, M.D. Ardema, Hypersonic Waverider Configuration from the 1950's to the 1990's, AIAA Paper 93-0774, 1993.
[3] K.G. Bowcutt, J.D. Anderson, D. Capriotti, Viscous optimized hypersonic waveriders, in: 25th AIAA Aerospace Sciences Meeting, 1987, p. 1987.
[4] S. Corda, J.D. Anderson, Viscous Optimized Hypersonic Waveriders Designed from Axisymmetric Flow Fields, AIAA Paper 88-0369, 1988.
[5] K.B. Center, H. Sobieczky, F.C. Dougherty, Interactive Design of Hypersonic Waverider Geometries, AIAA Paper 91-1697, 1991.
[6] K. Jones, K.B. Center, Waverider Design Methods for Non-Conical Shock Geometries, AIAA Paper 2002-3204, 2002.
[7] P.E. Rodi, The Osculating Flowfield Method of Waverider Geometry Generation, AIAA Paper 2005-0511, 2005.
[8] P.E. Rodi, D. Genovesi, Engineering Based Performance Comparisons Between Osculating Cone and Osculating Flowfield Waveriders, AIAA Paper 2007-4334, 2007.
[9] J.D. Anderson, Hypersonic and High-Temperature Gas Dynamics, 2nd ed., AIAA, Blacksburg, Virginia, 2006.
[10] W. Mason, J. Less, Aerodynamically blunt and sharp bodies, J. Spacecr. Rockets 31 (3) (1994) 378–382.
[11] T.F. O'Brien, M.J. Lewis, Power Law Leading Edges for Waveriders Designed with Shock Attachment, AIAA Paper 1998-0600, 1998.
[12] T.F. O'Brien, M.J. Lewis, Power law shapes for leading-edge blunting with minimal shock standoff, J. Spacecr. Rockets 36 (5) (sep. 1999) 653–658.
[13] W.F.N. Santos, Aerothermodynamic performance analysis of hypersonic flow on power law leading edges, J. Spacecr. Rockets 42 (4) (2005) 588–597.
[14] W.F.N. Santos, Bluntness effects on lift-to-drag ratio of leading edges for hypersonic waverider configurations, J. Spacecr. Rockets 46 (2) (2009).
[15] D.O. Vanmol, J.D. Anderson, Heat Transfer Characteristics of Hypersonic Waveriders with an Emphasis on Leading Edge Effects, AIAA Paper 1992-2920, 1992.
[16] M.J. Gillum, M.J. Lewis, Experimental results on a Mach 14 waverider with blunt leading edges, J. Aircr. 34 (3) (1997).
[17] K. Cui, S.-C. Hu, Shape Design to Minimize the Peak Heat-Flux of Blunt Leading-Edge, AIAA Paper 2013-0233, American Institute of Aeronautics and Astronautics, Grapevine (Dallas/Ft. Worth Region), Texas, 2013, pp. 1–14.
[18] P.E. Rodi, Optimization of Bezier Curves for High Speed Leading Edge Geometries, AIAA Paper 2013-1004, January 2013.
[19] T. Piskin, S. Eyi, Analysis and Adjoint Design Optimization of Hypersonic Blunt Bodies, AIAA Paper 2014-4022, 2014.
[20] T. Piskin, S. Eyi, M. Yumusak, Analysis and Design Optimization of Hypersonic Blunt Bodies, AIAA Paper 2014-40222, 2014.
[21] C. Seager, R.K. Agarwal, Shape Optimization of an Axisymmetric Blunt Body in Hypersonic Flow for Reducing Drag and Heat Transfer, AIAA Paper 2015-1704, 2015.
[22] P.E. Rodi, Integration of Optimized Leading Edge Geometries Onto Waverider Configurations, AIAA Paper 2015-1700, January 2015.
[23] K. Kontogiannis, A. Cerminara, N. Taylor, A. Soberster, N. Sandham, Parametric Geometry Models for Hypersonic Aircraft Components: Blunt Leading Edges, AIAA Paper 2015-3580, 2015.
[24] J.E. Johnson, R.P. Starkey, M.J. Lewis, Aerothermodynamic Optimization of Reentry Heat Shield Shapes for a Crew Exploration Vehicle, AIAA Paper 2006-6273, vol. 44, No. 4, 2006.
[25] J.E. Theising, Hypersonic Entry Aeroshell Shape Optimization, AE8900 MS Special Problems Report Space Systems Design Lab (SSDL), 2007.
[26] J.G. Meeroff, M.J. Lewis, R.P. Starkey, Computational Fluid Dynamics Solutions of Optimized Heat Shield Designs for Earth Entry, AIAA Paper 2009-7388, 2009.
[27] A.G. Neville, G.V. Candler, Computational-fluid-dynamics-based axisymmetric aeroshell shape optimization in hypersonic entry conditions, J. Spacecr. Rockets 52 (1) (2015).
[28] N.V. Queipo, R.T. Haftka, W. Shyy, T. Goel, R. Vaidyanathan, P. Kevin Tucker, Surrogate-based analysis and optimization, Prog. Aerosp. Sci. 41 (1) (2005) 1–28.
[29] A.I.J. Forrester, A. Sóbester, A.J. Keane, Multi-fidelity optimization via surrogate modelling, Proc. R. Soc. A, Math. Phys. Eng. Sci. 463 (2088) (2007) 3251–3269.

[30] A.I. Forrester, A.J. Keane, Recent advances in surrogate-based optimization, Prog. Aerosp. Sci. 45 (1–3) (2009) 50–79.
[31] C.G. Kyriakos, D.I. Papadimitriou, Adjoint methods for shape optimization, in: D. Thevenin, G. Janiga (Eds.), Optimization and Computational Fluid Dynamics, Springer, 2008, pp. 79–106.
[32] D.W. Zingg, M. Nemec, T.H. Pulliam, A comparative evaluation of genetic and gradient-based algorithms applied to aerodynamic optimization, Eur. J. Comput. Mech. 17 (1–2) (2008) 103–126.
[33] P.J. Roache, Quantification of uncertainty in computational fluid dynamics, Annu. Rev. Fluid Mech. 29 (1) (1997) 123–160.
[34] W. Kays, M. Crawford, B. Weigand, Convective Heat and Mass Transfer, 4th ed., McGraw–Hill, New York, NY, 2005.
[35] W.S. Hinman, C.T. Johansen, Rapid prediction of hypersonic blunt body flows for parametric design studies, Aerosp. Sci. Technol. 58 (2016).
[36] M.D. Salas, A Shock-Fitting Primer, Taylor & Francis Group LLC, Boca Raton, FL, 2010.
[37] J.A. Schetz, Boundary Layer Analysis, 1st ed., Prentice Hall, Upper Saddle River, New Jersey, 1993.
[38] C. Cohen, E. Reshotko, Similar Solutions for the Compressible Laminar Boundary Layer with Heat Transfer and Pressure Gradient, NACA TR 1293, 1956.
[39] OpenFOAM, OpenCFD Ltd., 2015.
[40] C.J. Greenshields, H.G. Weller, L. Gasparini, J.M. Reese, Implementation of semi-discrete, non-staggered central schemes in a colocated, polyhedral, finite volume framework, for high-speed viscous flows, Int. J. Numer. Methods Fluids 63 (1) (2009) 1–21.
[41] C. Arisman, C.T. Johansen, Nitric oxide chemistry effects in hypersonic boundary layers, AIAA J. 53 (12) (2015) 3652–3660.
[42] C. Arisman, C.T. Johansen, B. Bathel, P. Danehy, Investigation of gas seeding for planar laser-induced fluorescence in hypersonic boundary layers, AIAA J. 53 (12) (2015) 3637–3651.
[43] W.S. Hinman, C.T. Johansen, Interaction theory of hypersonic laminar near-wake flow behind an adiabatic circular cylinder, Shock Waves 26 (6) (2016) 717–727.
[44] E.J. Teh, C.T. Johansen, Effect of particle momentum transfer on an oblique-shock-wave/laminar-boundary-layer interaction, Acta Astronaut. 128 (2016) 431–439.
[45] X. Li, K. Wu, W. Yao, X. Fan, A comparative study of highly underexpanded nitrogen and hydrogen jets using large eddy simulation, Int. J. Hydrog. Energy 41 (9) (2016) 5151–5161.
[46] X. Li, W. Yao, X. Fan, Large-eddy simulation of time evolution and instability of highly underexpanded sonic jets, AIAA J. (May) (2016) 1.
[47] S. Reichel, R. Groll, Numerical simulation and experimental validation of a hypersonic flow for numerical modulation of re-entry phenomena prediction using adaptive mesh refinement, Int. J. Comput. Methods Exp. Meas. 1 (4) (2013) 381–394.
[48] NIST-JANAF, NIST-JANAF Thermochemical Tables, 2013.
[49] E. Rathakrishnan, Theoretical Aerodynamics, 1st ed., John Wiley & Sons Singapore Pte. Ltd., Singapore, 2013.
[50] M.H. Sohn, K.J. Lee, Bezier Curve Application in the Shape Optimization of Transonic Airfoils, AIAA Paper 2000-4523, 2000.
[51] J.A. Samareh, Survey of shape parameterization techniques for high-fidelity multidisciplinary shape optimization, AIAA J. 39 (5) (2001) 877–884.
[52] S. Eyi, M. Yumusak, Design Optimization in Hypersonic Flows, AIAA Paper 2012-5827, 2012.
[53] Matlab R2014a Optimization Toolbox, The Mathworks Inc., Natick Massachusetts, United States, 2014.